



**HAL**  
open science

## Hybrid polymeric micelles stabilized by gallium ions: Structural investigation

Stéphane Gineste, Barbara Lonetti, Marjorie Yon, Joanna Giermanska,  
Emanuela Di Cola, Michael Sztucki, Yannick Coppel, Anne-Françoise  
Mingotaud, Jean-Paul Chapel, Jean-Daniel Marty, et al.

► **To cite this version:**

Stéphane Gineste, Barbara Lonetti, Marjorie Yon, Joanna Giermanska, Emanuela Di Cola, et al..  
Hybrid polymeric micelles stabilized by gallium ions: Structural investigation. *Journal of Colloid and  
Interface Science*, 2022, 609, pp.698-706. 10.1016/j.jcis.2021.11.077 . hal-03630399

**HAL Id: hal-03630399**

**<https://hal.science/hal-03630399v1>**

Submitted on 6 Oct 2022

**HAL** is a multi-disciplinary open access archive for the deposit and dissemination of scientific research documents, whether they are published or not. The documents may come from teaching and research institutions in France or abroad, or from public or private research centers.

L'archive ouverte pluridisciplinaire **HAL**, est destinée au dépôt et à la diffusion de documents scientifiques de niveau recherche, publiés ou non, émanant des établissements d'enseignement et de recherche français ou étrangers, des laboratoires publics ou privés.

# Hybrid polymeric micelles stabilized by gallium ions: structural investigation

Stéphane Gineste<sup>a</sup>, Barbara Lonetti<sup>a</sup>, Marjorie Yon<sup>a</sup>, Joanna Giermanska<sup>b</sup>, Emanuela Di Cola<sup>c</sup>, Michael Sztucki<sup>d</sup>, Yannick Coppel<sup>e</sup>, Anne-Françoise Mingotaud<sup>a</sup>, Jean-Paul Chapel<sup>b</sup>, Jean-Daniel Marty<sup>a,\*</sup>, Christophe Mingotaud<sup>a,\*</sup>

<sup>a</sup> Laboratoire des IMRCP

CNRS UMR 5623, University of Toulouse, Université Toulouse III - Paul Sabatier  
118, route de Narbonne 31062 Toulouse Cedex 9, France

<sup>b</sup> Centre de Recherche Paul Pascal

CNRS UMR 5031, University of Bordeaux,  
115, Avenue du Dr Albert Schweitzer 33600 Pessac, France

<sup>c</sup> SAS-analysis.eu, 38120 Saint Egrève, France

<sup>d</sup> European Synchrotron Radiation Facility

71, avenue des Martyrs, CS 40220, 38043 Grenoble Cedex 9, France.

<sup>e</sup> Laboratory of Coordination Chemistry, CNRS UPR 8241, University of Toulouse, 205 route de Narbonne, 31077 Toulouse, France

\* Corresponding authors:

E-mail addresses: [christophe.mingotaud@univ-tlse3.fr](mailto:christophe.mingotaud@univ-tlse3.fr) (C. Mingotaud) and [jean-daniel.marty@univ-tlse3.fr](mailto:jean-daniel.marty@univ-tlse3.fr) (J.-D. Marty)

## ABSTRACT

The addition of gallium ions to a solution of a double-hydrophilic block copolymer, i.e. poly(ethylene oxide)-*block*-poly(acrylic acid), leads to the spontaneous formation of highly monodisperse micelles with a Hybrid Polyion Complexes (HPICs) core. By combining several techniques, a precise description of the HPIC architecture was achieved. In particular and for the first time, NMR and anomalous small angle X-ray scattering (ASAXS) enable tracking of the inorganic ions in solution and highlighting the co-localization of the gallium and the poly(acrylic acid) blocks in a rigid structure at the core of the micelle. Such a core has a radius of ca 4.3 nm while the complete nano-object with its poly(ethylene oxide) shell has a total radius of ca 11 nm. The aggregation number was also estimated using the ASAXS results. This comprehensive structural characterization of the Ga HPICs corroborates the assumptions made for HPICs based on other inorganic ions and demonstrates the universality of the HPIC structure leading, for example, to new families of contrast agents in medical imaging.

## KEYWORDS

Polyion, ASAXS, micelle, polymer, gallium

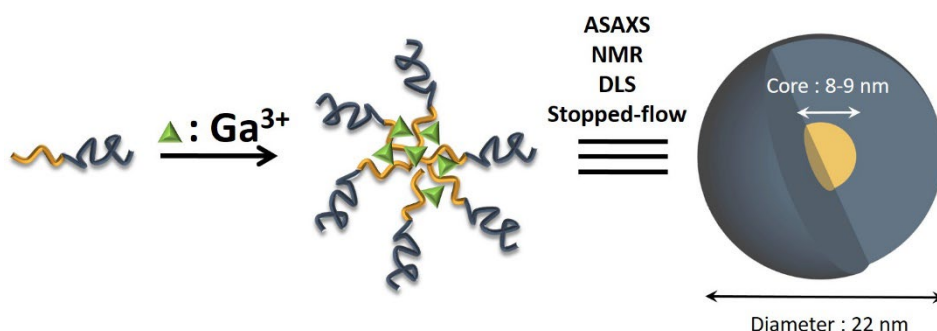
## ABBREVIATIONS

HPIC, hybrid polyion complex; PEO, poly(ethylene oxide); PAA, poly(acrylic acid); ASAXS, anomalous small angle X-ray scattering; DLS, dynamic light scattering

## CRedit AUTHOR STATEMENT

**Stéphane Gineste:** Resources, Investigation, Writing - Review & Editing **Barbara Lonetti:** Investigation, Writing - Original Draft **Marjorie Yon:** Investigation, Writing - Review & Editing **Joanna Giermanska:** Investigation, Writing - Review & Editing **Emanuela Di Cola:** Formal analysis, Writing - Original Draft **Michael Sztucki:** Investigation, Formal analysis, Writing - Original Draft **Yannick Coppel:** Investigation, Formal analysis, Writing - Original Draft **Anne-Françoise Mingotaud:** Investigation, Writing - Review & Editing **Jean-Paul Chapel:** Investigation, Writing - Review & Editing **Jean-Daniel Marty:** Funding acquisition, Writing - Review & Editing **Christophe Mingotaud:** Conceptualization, Investigation, Writing - Original Draft.

## GRAPHICAL ABSTRACT



## INTRODUCTION

Self-assembly of amphiphilic compounds such as surfactants or copolymers has been the focus of numerous studies for several decades. Micelles, worm-like micelles, vesicles, lyotropic phases etc. were then applied to various fields ranging from material science to medicine.[1-4] Such assemblies are formed thanks to the hydrophobic effect.[5] It is less energetically costly for the solvent (i.e. water) to interact with the hydrophilic surface of aggregates whose hydrophobic parts are hidden from water, than to individually solvate free amphiphilic molecules or macromolecules. Beyond this hydrophobic effect, purely hydrophilic compounds may also self-associate. For instance, complex coacervates are formed thanks to electrostatic interactions between oppositely charged macromolecules.[6-8] Coulombic interactions combined with an entropy gain resulting from the release of counterions (and bound water molecules) explain the formation of micelles, vesicles and more or less dense nanoparticles with typical sizes of few tens to hundreds of nanometers.

Among all the natural or synthetic hydrophilic polymers generating aggregates, double hydrophilic block copolymers (DHBCs) have gained increasing attention.[9, 10] Typically, a neutral block (such as poly(ethylene glycol)) is linked to a second block which can be either neutral (e.g. poly(vinylalcohol...)) or ionic (e.g. poly(acrylic acid), poly(2-(diethylamino)ethyl methacrylate...)). In the presence of a polymer of the opposite charge, the DHBC will form micellar polyelectrolytes.[11] Instead of a second charged polymer, metal ions can be used to generate coulombic interactions. For example, K. Kataoka and coll. analyzed mixtures of platinum ions with poly(ethylene glycol)-*block*-poly(aspartic acid) copolymers.[12] Aluminum,[13, 14] manganese,[13, 15] iron,[16] copper,[14] zirconium,[17] or lanthanides[14, 17, 18] were later studied. In such systems, coulombic interactions and complexations between the metal centers and polymer functions (acting as ligands) are responsible for DHBC aggregation.

The choice of the metal ion is often motivated by the expected final property of these hybrid polyion complexes (HPICs) in material or medical science. However, the complete characterization of these nano-objects is often difficult and, in particular, the localization of the metal ions in the HPIC structure is more deduced than demonstrated. We thus put under scrutiny a copolymer – metal ions system and use a set of complementary techniques to get a precise characterization of the hybrid structure. Two main techniques can help tracking the metal ions in the ion-copolymer mixtures: Nuclear Magnetic Resonance (NMR) if the nucleus of the metal ion is compatible, and Anomalous Small-Angle Scattering of X-rays (ASAXS) if the absorption edge of the metal ion is in the right energy range. Gallium is one of the few elements that meet the above criteria. Furthermore, it can be easily obtained as stable aqueous trivalent ions.

In this paper, we report the formation and the characterization (notably by NMR and ASAXS, but also by multi-angle dynamic light scattering – DLS) of Ga HPICs using poly(ethylene oxide)-*block*-poly(acrylic acid) PEO<sub>5k</sub>-PAA<sub>3.2k</sub> following the process described in **Figure 1**. We demonstrate that this formulation pathway is fast and leads to weakly polydisperse nano-objects in which the gallium ions are trapped.

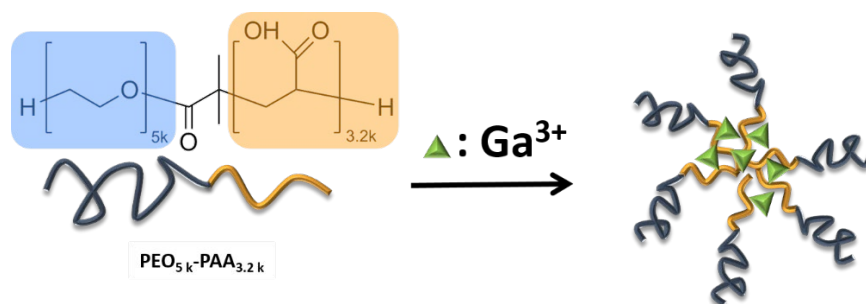


**Figure 1:** Molecular structure of the PEO<sub>5k</sub>-PAA<sub>3.2k</sub> diblock copolymer and scheme of the HPICs formation triggered by the addition of gallium ions to a PEO<sub>5k</sub>-PAA<sub>3.2k</sub> polymer solution.

## MATERIALS AND METHODS

### Chemicals

$\text{Ga}(\text{NO}_3)_3 \cdot 6\text{H}_2\text{O}$  was purchased from Sigma Aldrich Co., Ltd. at highest purity available (99.9%) and used as received.  $\text{PEO}_{5k}\text{-PAA}_{3.2k}$  was purchased from Polymer Source™ and used as received. Its PDI is estimated around 1.1 (1.05 for the poly(ethylene oxide block alone)) by the supplier (see **Data Sheet S1** in the Supplementary Information). The size of this copolymer was chosen as close as possible to the one used in a previous publication.[18] Water was purified through a filter and ion exchange resin using a Purite device (resistivity 18.2  $\text{M}\Omega\cdot\text{cm}$ ).

### HPICs solutions

A HPIC solution was prepared with  $\rho = 3 \cdot [\text{Ga}^{3+}]/[\text{AA}] = 1$  by adding an appropriate amount of a  $\text{Ga}(\text{NO}_3)_3$  stock solution to an aqueous solution of  $\text{PEO}_{5k}\text{-PAA}_{3.2k}$ . The pH of the final mixture was possibly adjusted if required by dropwise addition of NaOH (1 M) or HCl (1 M). The final polymer concentration in the mixture was 0.1 wt%.

For (A)SAXS experiments, more concentrated solutions were used with the concentration of  $\text{Ga}^{3+}$  kept constant ( $c = 10 \text{ mM}$ ) while varying the  $\text{PEO}_{5k}\text{-PAA}_{3.2k}$  content (up to 10 wt%). pH was adjusted to  $7.0 \pm 0.2$ .

### Stopped flow light scattering technique

Stopped flow (SF) light scattering experiments were performed on a Bio-Logic SFM 400 stopped-flow module equipped with a MOS 450 spectrometer, MPS70/4 syringe controller, PMS 450 photodetector and BioKine software. The mixing module contained four independent 10 mL syringes driven by independent stepping motors. Syringe 1 contained the  $\text{PEO}_{5k}\text{-PAA}_{3.2k}$  solution, syringe 2 the Ga salt solution, syringes 3 and 4 pure water. Mixing was performed using a Berger Ball mixer to create turbulence under the most stringent conditions. An FC-15 cuvette was used as the sample cell. The hard stop was installed on top of the observation head. The flow rate was set to  $9.1 \text{ mL}\cdot\text{s}^{-1}$ , which resulted in a dead time of 4.1 ms. Scattered light at a wavelength of 438 nm was recorded at  $90^\circ$  using the PMT detector. The voltage applied to the detector was adjusted according to the signal intensity to avoid saturation. It was set at 420V. For each mixing charge ratio  $\rho$ , three injections of water (syringe 3) were performed in a row to flush the cuvette. Three injections of the mixture (syringe 1 and 2) were then performed and averaged to obtain the complexation kinetics. The standard deviations were found around 1.6%, 0.4%, 0.5% and 5% of the measured intensities, respectively for  $\rho = 0.6, 0.8, 0.9$  and 1.

### NMR experiments

NMR experiments were recorded in  $\text{D}_2\text{O}$  at 298K on a Bruker Avance 600 NEO spectrometer equipped with a 5 mm triple resonance inverse Z-gradient probe (TBI 1H, 31P, BB). 15 s relaxation delays were used to obtain reliable  $^1\text{H}$  integration data (estimated error  $\text{ca} \pm 3\%$ ). The  $T_1$  spin-lattice relaxation times (estimated error  $\text{ca} \pm 5\%$ ) were measured by the inversion recovery method.  $^{71}\text{Ga}$  spectra were acquired with an acquisition time of 50 ms and a recycle delay of 50 ms. All chemical shifts for  $^1\text{H}$  and  $^{71}\text{Ga}$  are relative to TMS and  $\text{Ga}(\text{NO}_3)_3$ , respectively. One series of 12 samples with various gallium/polymer ratios has been analyzed.

### Dynamic light scattering

Multi-angle dynamic light scattering (DLS) experiments were performed on a 3D LS spectrometer from LS instruments (Switzerland) at  $25^\circ\text{C}$ . Working with a laser at 660 nm, this instrument recorded the light scattered at angles between  $15$  and  $150^\circ$  (typically more than  $\text{ca} 60$  values). Typical acquisition time for each angle was set to 30 s. Five correlograms were recorded for each angle. All DLS data were then analyzed using a laboratory made software program (named M-STORMS).[4] Cumulant or NNLS (Non-Negative Least Squares) method led to an estimation of the decay rate  $\Gamma$  for each angle. The linear dependency of  $\Gamma$  versus the square of the scattering

vector  $q$  ( $\Gamma = q^2 \cdot D$ ) gives the diffusion coefficient of the nano-objects and therefore their radius through the Stokes-Einstein equation:  $D = \frac{k \cdot T}{6\pi\eta \cdot R_h}$  where  $T$  is the temperature and  $\eta$  the viscosity of the solution.

Generally, the correlograms of HPICs solution correspond to a simple narrow distribution in size (around 10-20 nm). Rarely, for low angles, a second peak (around 100-150 nm) was detected which disappears after a simple filtration of the solutions. When present, the concentration of such larger objects was near or less than  $10^{-4}$  % in number of the HPICs concentration. Size error was estimated by the standard deviation of all the calculations (with cumulant and NNLS methods, ca 10-12 values per experiment) for all similar experiments (4 experiments).

Mono-angle dynamic light scattering measurements were conducted using a Zetasizer Nano-ZS (Malvern Instruments, Ltd, UK) with integrated 4 mW He-Ne laser at  $\lambda = 633$  nm. Light scattering intensity (at  $173^\circ$ ) was measured with instrumental parameters set to constant values for all the samples. The correlation function (measured twice for each sample) was analyzed *via* the cumulant method to get the Z-average size of the colloids. Standard deviation in the intensity and Z-average size are found for each sample respectively around 10% and 5%.

### Small-Angle and Anomalous Small Angle X-ray Scattering

Small-Angle X-ray Scattering (SAXS) measurements were performed at the high brilliance ID02 beamline of the European Synchrotron (ESRF, Grenoble, France).[19] The 2D SAXS patterns were collected using a Rayonix MX-170HS ccd detector. A sample-to-detector distance of 1 m was employed in order to cover a  $q$ -range,  $2 \times 10^{-2} < q < 2 \text{ nm}^{-1}$  where  $q$  is the scattering wave vector defined as  $q = (4\pi/\lambda) \sin \vartheta/2$ ,  $\lambda$  being the wavelength ( $\lambda \sim 1.2 \text{ \AA}$ ) close to the K absorption edge of Gallium and  $\vartheta$  the scattering angle. Measurements were performed in a flow through quartz capillary (diameter of about 1.8 mm) which allows a reliable background subtraction and to exclude radiation induced by the x-ray exposure by refreshing the sample. The measured two-dimensional SAXS patterns were corrected for detector artefacts, normalized to absolute intensity scale and azimuthally averaged to obtain the intensity profile  $I(q)$  as a function of  $q$  using standard procedures.[20] The background scattering was subtracted from each averaged sample intensity profile using the SAXSutilities analysis package.[21] These measurements were performed on one series of samples with different gallium/polymer concentration ratios. The error of the SAXS measurements shown in Figure 6 is basically covered by the size of the symbols. For the ASAXS measurements shown in Figure 7, just the relative intensity variation as a function of X-ray energy is meaningful. Also for this case the statistical error is within the size of the symbols shown in the insets.

The SAXS background-subtracted scattered intensity  $I(q)$  can then be expressed as:

$$I(q) = NV^2 \Delta\rho_{sl}^2 P(q)S(q) \quad (\text{Eq. 1})$$

where  $N$  is the number of particles per unit volume  $V$ ,  $\Delta\rho_{sl}$  is the difference in the scattering length densities (SLD) between the particles and the medium,  $P(q)$  and  $S(q)$  are the form and the structure factors, describing the shape and interaction between particles, respectively.

The low- $q$  region (plateau) of the data set can be used to derive the gyration radius,  $R_g$ , according to the Guinier analysis using the expression:

$$I(q) = I_0 \exp\left(\frac{-R_g^2}{3} q^2\right) \quad (\text{Eq. 2})$$

allowing estimating the overall size of the particles.[22]

The SAXS intensity profiles were modelled using the form factor of polydisperse spherical core-shell particles  $P(q)_{cs}$ , assuming that the structural factor  $S(q)$  is close to 1 (low concentration).

$$P(q)_{cs} = \left[ V_c \Delta\rho_{cs} \frac{\sin(qR_c) - qR_c \cos(qR_c)}{(qR_c)^3} + V_e \Delta\rho_{sm} \frac{\sin(qR_e) - qR_e \cos(qR_e)}{(qR_e)^3} \right]^2 \quad (\text{Eq. 3})$$

$V_c$  and  $V_e$  indicate the volumes of core and whole particle,  $R_c$  the radius of the core,  $R_e$  is the external radius, and  $\Delta\rho_{cs}$ ,  $\Delta\rho_{sm}$ , are the relative scattering length density differences between core (PAA) - shell (PEO) and shell (PEO) - medium (solvent), respectively.

An additional contribution describing the spatial fluctuations of the polymer chains was also added to model the high- $q$  behavior of the scattering data (Ornstein-Zernike term). Therefore, the total SAXS intensity  $I(q)$  is described as:

$$I(q) = P(q)_{cs} + I(q)_{OZ} \quad \text{(Eq. 4)}$$

where  $I(q)_{OZ} = \frac{I_0}{(1+\xi^2q^2)^d}$  with  $\xi$  the internal correlation length and  $d$  the fractal exponent which was fixed to -1.6 as expected for swollen polymer chains in good solvent.

Complementary to SAXS, anomalous small angle X-ray scattering (ASAXS) measurements were performed, by tuning the x-ray energy close to the Gallium K-edge. As described in detail in the literature, such technique enables element specific contrast variation and hence the possibility to determine the spatial location of the  $\text{Ga}^{3+}$  counterions.[23, 24] The contrast variation in ASAXS is given by the energy dependence of the relative atomic scattering factor  $\Delta f(E)$ :

$$\Delta f(E) = \Delta f_0 + f'(E) + if''(E) \quad \text{(Eq. 5)}$$

where the non-resonant term  $f_0$  is the atomic number of the element,  $f'$  and  $f''$  are the real and imaginary part of  $f$  as a function of the incident x-ray energy  $E$ .

As a result, the energy dependence of the radial scattering length density profile  $\Delta\rho_{SL}$  can be calculated as:

$$\Delta\rho_{SL}(r, E) = v(r) r_e \Delta f(E) = \Delta\rho_{SL}^0(r) + v(r) r_e [f'(E) + if''(E)] \quad \text{(Eq. 6)}$$

with  $v(r)$  being the spatial distribution of the anomalous scattering units (i.e. Ga ions),  $r_e$  the classical electron radius and  $\Delta\rho_{SL}^0(r)$  the non-resonant scattering length density profile (i.e. the usual contrast well below the absorption edge).

Therefore, the total scattering intensity  $I(q, E)$  can be expressed as follows:

$$I(q, E) = F_0^2(q) + 2f'(E)F_0(q)v(q) + [f'(E)^2 + f''(E)^2v^2(q)] \quad \text{(Eq. 7)}$$

where the term  $F_0^2(q)$  denotes the non-resonant intensity, depending on the total electron density of the material,  $v^2(q)$  is the energy dependent resonant term which denotes the counterion ( $\text{Ga}^{3+}$ ) self-contribution and  $F_0(q)v(q)$  is the cross-term, containing information about both the resonant and non-resonant terms. The energy dependence of the atomic scattering factors close to the  $\text{Ga}^{3+}$  K-edge is shown in **Figure S1**. For ASAXS experiments, SAXS patterns were collected at different energies below and above the  $\text{Ga}^{3+}$  absorption edge ( $\Delta E = -117, -47, -27, -11, -3, -1, +1, +13$  and  $+53$  eV).

A first data analysis of the ASAXS data was done by decomposing the measured data in the three partial intensities according to Eq. 6 (see discussion in the according paragraph).

To derive even more details about the spatial distribution of the counterions and to assess the density of the gallium ions in the system, quantitative model fitting of the ASAXS curves was performed using an analytic model developed as plugin in the SAXSutilities package [23]. Based on the qualitative results by decomposition, as the partial intensities according to Eq. 7 show a similar intensity distribution for the energy independent SAXS term and the contribution originating from the counterions (see text for more details), the model used for the fitting of ASAXS curves assumes the counterions distribution to be arranged in a similar core-shell structure as  $\text{PEO}_{5k}\text{-PAA}_{3.2k}$ . Moreover, by analogy with the work of Dingenouts, et al.,[25] an Ornstein-Zernike term (OZ) was added to simulate the high- $q$  tail contribution of the density fluctuation not only in the distribution of PEO/PAA but also in the counterions distribution. The OZ term in the latter case scales according to the energy dependent contrast variation of the  $\text{Ga}^{3+}$  counterions.

Therefore, the total ASAXS intensity  $I(q, E)$  is described as:

$$I(q, E) = P(q)_{cs} + I(q)_{OZ} + P(q, E)_{cs, Ga} + I(q, E)_{OZ, Ga} \quad \text{(Eq. 8)}$$

$P(q)_{cs}$  uses the relative scattering length density differences of PAA, PEO and solvent according to **Eq. 3**, whereas  $P(q, \Delta E)_{cs, Ga}$  uses in the same equation the radial scattering length density profile based on the spatial distribution of Ga ions according Eq. 6. It should be emphasized, that all contributions in **Eq. 8** use the same unique set of structural parameters derived already from the SAXS analysis for fitting the scattering curves recorded at different energies. One should emphasize that all contributions to **Eq. 8** use the same and unique set of (1) structural parameters derived already from the SAXS analysis and (2) the density of the Ga ions in the core and the shell (see **Table S1**) for fitting the scattering curves recorded at different energies. Only the scattering contrast of the Ga ions varies according to **Eq. 5**. Due to its higher complexity, the polydisperse model needs to be calculated numerically (taking into account a size distribution of the core).

## RESULTS AND DISCUSSION

### Formation of the Ga HPICs

To an aqueous solution of the PEO<sub>5k</sub>-PAA<sub>3.2k</sub> block copolymer, various amounts of a concentrated solution of gallium nitrate were added in order to adjust the charge ratio,  $\rho$ , between the positive and negative charges of the gallium ions and the ionized or ionizable carboxylic functions of the PAA block respectively:

$$\rho = \frac{3.[Ga^{3+}]}{[AA]} \quad (\text{Eq. 9})$$

At charge stoichiometry, when  $\rho$  is equal to 1, the fully ionized PAA chains are theoretically electroneutralized by the gallium ions. The final polymer concentration in the different mixtures was kept constant and equal to 0.1 wt%. The gallium/polymer solutions were then analyzed by light scattering. A solution of pure PEO<sub>5k</sub>-PAA<sub>3.2k</sub> block copolymer is characterized by a very weak scattered intensity and the corresponding correlogram is associated to a Z-average size above 100 nm. This was supposedly due to traces of poorly defined self-associations of the copolymers.[18] As suggested in a M. Muthukumar's paper, such associations may have a microgel-like structure "where the physical cross-links arise from dipole-dipole pairings with each dipole originating from an adsorbed counterion to a charged monomer belonging to the polymer".[26]

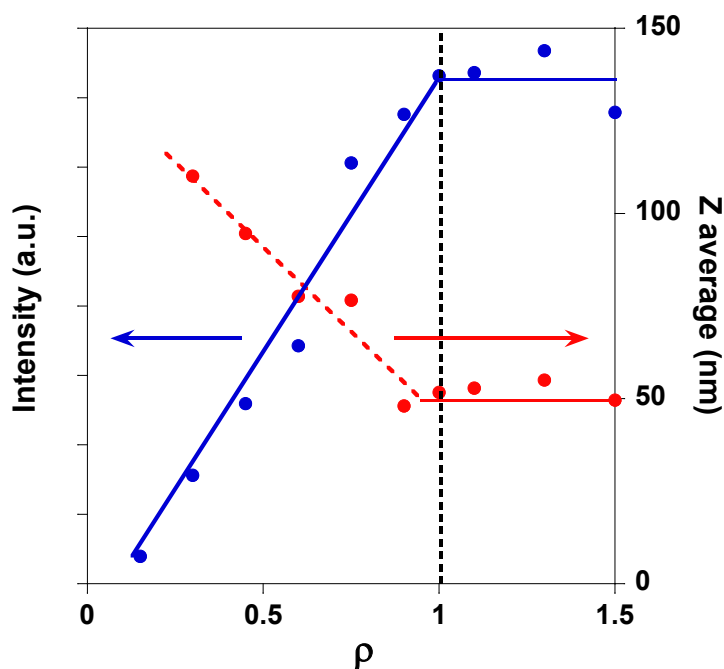


**Figure 2:** Typical evolutions of the scattered light intensity (in blue) and Z-average size (diameter in nm, in red) measured by a mono-angle DLS instrument from gallium/ PEO<sub>5k</sub>-PAA<sub>3.2k</sub> mixtures versus the ratio  $\rho$ . The lines are



just a guide for the eyes. Because of self-assembly of the polymers existing initially in the pure copolymer solution, the Z-average size obtained for  $\rho$  below ca 0.9 corresponds to polydisperse nano-objects (symbolized by the dashed red line). Above  $\rho \sim 0.9$ , the size distribution is mono-modal.

As shown in **Figure 2**, the intensity of the scattered light increases with gallium amount. This increase is more or less linear with  $\rho$  up to 1. Above 1, the intensity is approximately constant (or slightly decreasing). Such evolution suggests that objects containing several macromolecules were formed by addition of the gallium ions until electroneutrality was reached. Analysis of the DLS correlograms reveals a polydisperse population of objects in the solution for  $\rho$  lower than ca 0.9. The ill-defined copolymer aggregates present in the initial solution as impurities/micro-gel ( $\rho=0$ ) are subsequently disaggregated by gallium ions that interact strongly with carboxylate groups, resulting in an apparent z value that decreases to  $\rho=1$ . This led to a clean mono-modal population for  $\rho$  close to or higher than 1. Such evolution can be followed as a function of the Z-average diameter of the particles, for which a clear breaking in the slope versus the ratio  $\rho$  is recorded around unity. Well-defined polymeric nanoparticles were then formed by addition of gallium ions. Such a behavior is similar to that described with gadolinium ions and a similar copolymer.[18] Before any structural analysis of these hybrid polymer micelles, a good knowledge of the aggregation kinetics is necessary to avoid any artifact due to the metastability of the mixtures. Stopped-flow experiments were then undertaken. The fast mixing of gallium and copolymer solutions at different charge ratios  $\rho$  was monitored as a function of time by light scattering.

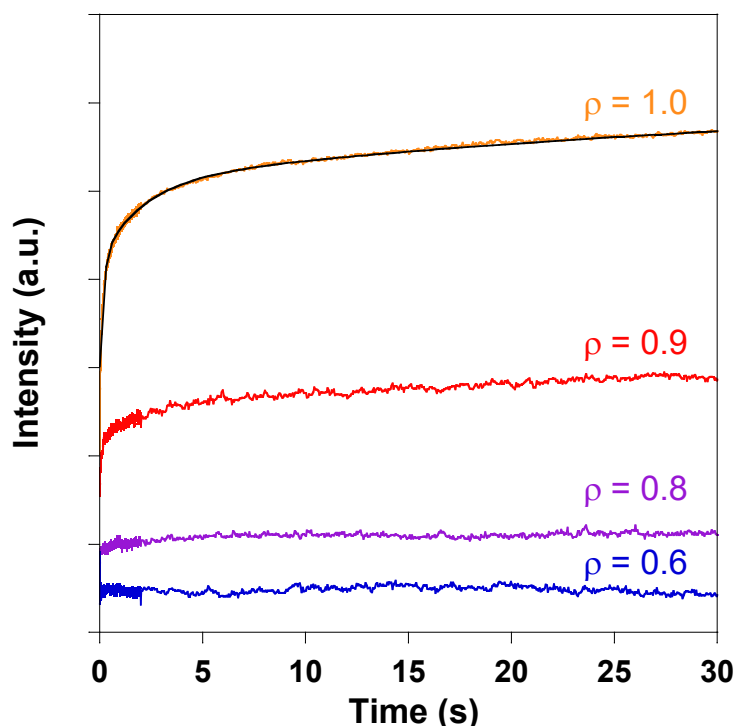


**Figure 3:** HPIC complexation kinetics monitored by stopped-flow experiments. The flow rates of gallium and copolymer stock solutions were adjusted to be equivalent for the different charge ratios  $\rho$ . The solid black line is an example of fitting the data for  $\rho = 1$  with three exponential decays.

As shown in **Figure 3** and in agreement with **Figure 2**, the overall scattered intensity increases with  $\rho$  toward unity. The stabilization of the scattered intensity versus time is very fast below 0.8. When  $\rho$  is close to 1, a neat increase of the intensity is observed. The data were then modeled by multi exponentially decaying functions giving rise to characteristic times that are not modified by the charge ratio  $\rho$ . Average values and standard deviations (calculated for experiments with  $\rho$  equal to 1 and 0.9) were then extracted: ca  $0.08 \pm 0.01$  s

(associated to ca 0.4% of the signal),  $1.8 \pm 0.2$  s (ca 4% of the signal) and  $39 \pm 1$  s (ca 95% of the signal). The first two shorter times likely correspond to a monomodal but relatively broad distribution of characteristic times as discussed in Kuehn et al.[27]. The longest characteristic time, which accounts for more than 95% of the signal, is equivalent to that measured during the formation of polyelectrolyte complex micelles. It may be related to the compositional equilibration of the HPICs by exchanging either unimers or ions. The first two smaller times are shorter compared to those measured in the aggregation of two polyions that may well describe the formation of metastable pre- or large scale aggregates.[27] Whatever the exact process associated with these characteristic times may be, the average kinetic constant of such process is  $0.2 \pm 0.02$  s. This suggests that both ions and copolymers reached a pseudo-equilibrium quickly after mixing. This was confirmed by DLS data, which showed no significant changes in the scattering properties of the solution between a few minutes and a few days. Furthermore, from these stopped-flow experiments we can hypothesize that polymer aggregates with  $\rho$  close to 1 and below 0.7-0.8 might not have the same morphology. Such interpretation is also supported by SAXS data (see below) and DLS experiments (see **Figure S2**).

To get more information on the formation of the hybrid aggregates,  $^1\text{H}$  NMR experiments were performed. As depicted on **Figure 4A**, while the peaks related to PEO units around 3.7-3.3 ppm remained roughly constant with  $\rho$ , the ones associated to the carboxylate functions at 2.3-1.9 and 1.7-1.4 ppm (respectively due to the hydrogen in  $\alpha$  and  $\beta$  of the carboxylate functions) progressively disappeared when  $\rho$  increased. The longitudinal relaxation time ( $T_1$ ) of the proton that can be associated with the mobility of molecular chains was measured (**Figure 4B**). It was observed that  $T_1$  of protons in  $\beta$  position at 1.32 ppm of carboxylate units remained constant at ca. 100 ms for ratio below 0.75 and then rapidly increased to reach 2000 ms for  $\rho = 2$ . The evolution of  $T_1$  evidenced the formation of HPICs for ratio above 0.75 with restricted motion of polymer chains. Below this value, no aggregation was evidenced and the polymer roughly behaved as isolated or poorly associated chains. These  $T_1$  values were further taken into account to acquire  $^1\text{H}$  NMR spectra in quantitative conditions and to determine the evolution of the integral ratio of the proton associated to the carboxylate unit to the PEO unit (**Figure 4B**).

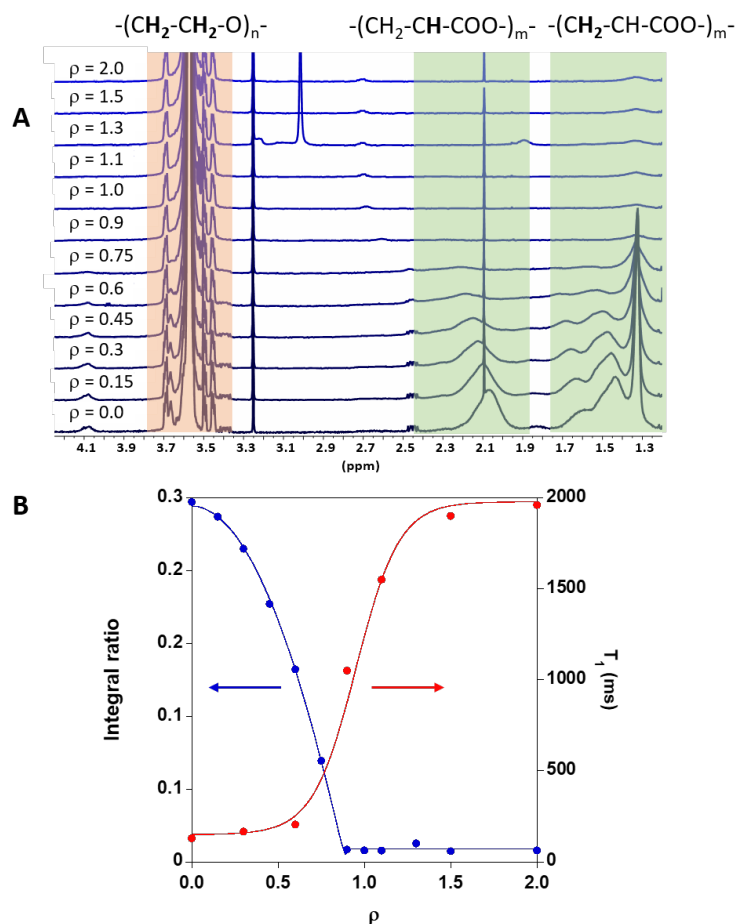


**Figure 4:** **A)** Evolution of  $^1\text{H}$  NMR spectra of HPIC solutions (in  $\text{D}_2\text{O}$ , 298 K) as a function of  $\rho$ . **B)** Evolution of the integral ratio (in blue) of the proton associated to the carboxylate unit to the PEO unit and  $T_1$  (in red) as a function of  $\rho$  deduced from NMR spectra.  $T_1$  was measured on the carboxylate signal at 1.32 ppm.

Concomitant with the observed evolution of  $T_1$ , the integral ratio decreased for ratios above 0.75 corresponding mainly to the disappearance of the signal arising from hydrogen near the carboxylate units. The selective suppression of these peaks suggested the preferential  $\text{Ga}^{3+}$  binding on PAA residues as expected from the intrinsic chelating capability of acrylates and the rigidification of the PAA blocks. Indeed, the NMR signal disappearance is due to a strong broadening of the NMR resonances associated to very short  $T_2$  transverse relaxation times caused by slow local tumbling motions. Meanwhile, integration relative to PEO chains only slightly evolved suggesting a higher mobility of these chains in aqueous solution. This might be ascribed to the formation of HPICs with a core-shell structure with a PAA/Ga core surrounded by PEO chains.

The interaction of  $\text{Ga}^{3+}$  with the polymers was further evidenced by  $^{71}\text{Ga}$  NMR analysis (**Figure S3**). Gallium has two NMR active quadrupolar nuclei (spin  $I=3/2$ ):  $^{69}\text{Ga}$  and  $^{71}\text{Ga}$ ; the latter being more sensitive and producing narrower signals despite a lower natural abundance.  $^{71}\text{Ga}$  NMR signal can only be observed when  $\text{Ga}^{3+}$  ions are in a cubic or octahedral symmetric local environment because its strong quadrupolar moment leads to very broad signal in the other cases. In aqueous solution, only the octahedral  $[\text{Ga}(\text{H}_2\text{O})_6]^{3+}$  and the tetrahedral  $[\text{Ga}(\text{OH})_4]^-$  can thus be observed among the different species.[28] Hence, whereas pristine free  $\text{Ga}^{\text{III}}$  solutions gave a peak at 0.3 ppm corresponding to the hexa - aqua ion,  $[\text{Ga}(\text{H}_2\text{O})_6]^{3+}$ , this peak disappeared for ratio  $\rho$  lower than 1, indicating that  $\text{Ga}^{\text{III}}$  ions were no longer available to form such highly symmetric species due to interactions with PAA and/or were trapped within the HPIC structure.

## Characterization of the size and structure of the Ga HPICs

The size of the HPICs formed by the gallium ions was estimated using DLS. The correlograms measured (see insert of **Figure 5**) were perfectly fitted using the cumulant method. This is a direct evidence for the narrow size dispersion of the HPICs. Generally, NNLS analysis confirmed the narrow size distribution (around 10-20 nm). Rarely, for low angles, a second peak (around 100-150 nm) was detected, which often disappeared by a simple filtration of the samples. When present, the concentration of such larger objects was close to or less than  $10^{-4}\%$  of the HPICs concentration.

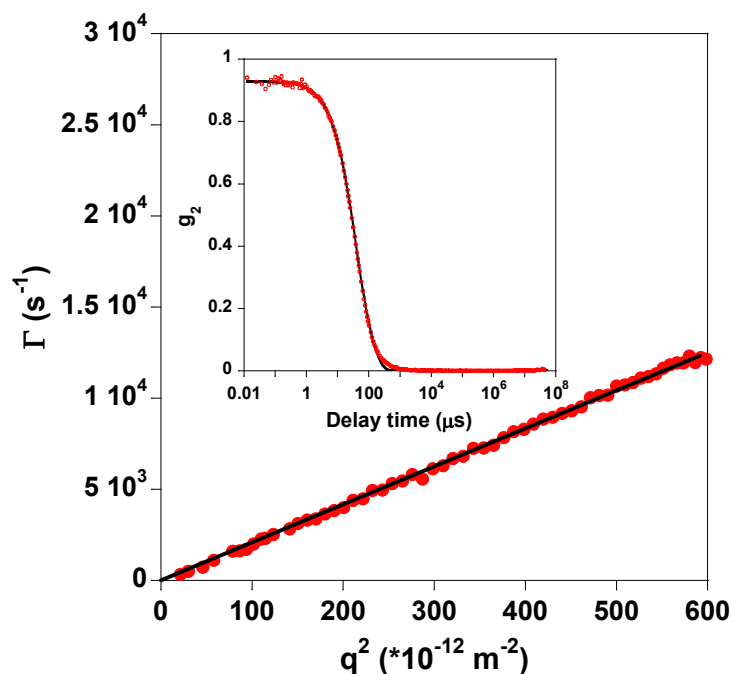


**Figure 5:** Analysis of typical multi-angle DLS data for a Ga HPIC solution ( $\rho = 1$ ). Decay rate  $\Gamma$ , estimated using the cumulant method, versus the scattering vector  $q$ . **Insert:** Typical  $g_2$  correlogram (red circles) obtained for a Ga HPIC solution at a scattering angle of  $148^\circ$ . In black, best fit using the cumulant method (second order) with the M-STORMS software.

Multi-angle DLS experiments were then performed in order to get the best possible accuracy on the hydrodynamic size of the Ga HPICs. As shown in **Figure 5**, the dependence of  $\Gamma$  with the square of the scattering vector  $q$  is linear, demonstrating that the HPIC nano-objects exhibited a Brownian motion. The slope of  $\Gamma$  versus  $q^2$  gave the diffusion coefficient of the nano-objects and thus their radius through the Stokes-Einstein equation. From these data, an average hydrodynamic radius of  $11 \pm 3$  nm was obtained for the Ga HPICs (see **Table 1**). This size is quite in line with that obtained for gadolinium or copper HPICs (respectively  $11.5 \pm 1.2$  nm and  $14.5 \pm 2$  nm).[17, 29]

To get detailed information on the HPIC internal structure, SAXS experiments were performed on HPIC solution. Firstly, SAXS structural investigations were performed on the mixtures of gallium and PEO<sub>5k</sub>-PAA<sub>3.2k</sub> polymer at different ratios  $\rho$  with the gallium concentration being constant. As shown in **Figure 6**, the SAXS scattering signal for  $\rho$  below 0.8 resembles that of the pure copolymer. Above this value, the forward scattered intensity increased until the electroneutrality was reached. Above  $\rho = 1$ , the further decrease of polymer (or increase of gallium ion) concentration had no effect (not shown). Such a behavior is in total agreement with the DLS and stopped-flow experiments. Therefore, for  $\rho$  below ca 0.6-0.8, nano-objects formation is not detected and electrostatic interactions between charged PAA chains are the dominant feature of the SAXS scattering curves partially screened by gallium ions interacting with the macromolecules. Indeed, approaching the electroneutrality, the electrostatic repulsions were fully screened and nano-objects with an average radius of gyration  $R_g$  of 7.5 nm were formed (see **Table 1**).

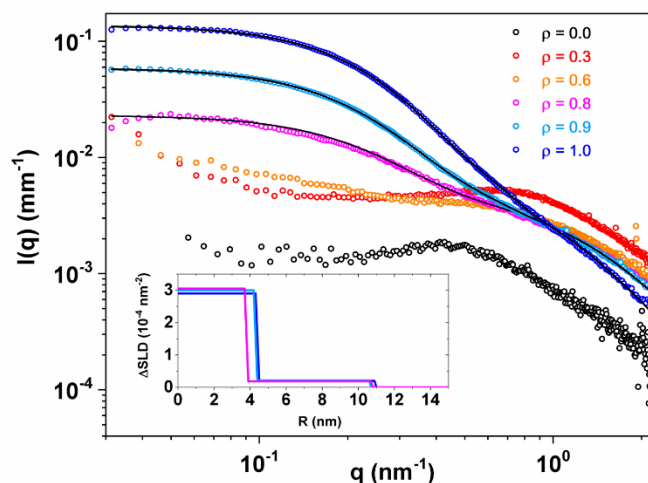


**Figure 6:** Evolution of the SAXS scattering signal of gallium-copolymer solutions as a function of the ratio  $\rho$  at a fixed  $\text{Ga}^{3+}$  concentration of 10 mM. Solid lines: best fitting according to Eq. 4 of the SAXS scattering signal of Ga HPICs solution with  $\rho$  from 0.8 to 1. For clarity, only 10% of the experimental points are plotted. **Insert:** The electron density profiles ( $\Delta\text{SLD}$ ) for the core-shell particle deduced from the best fittings.

The ratio  $R_g/R_h$  is found around 0.68, a lower value than the theoretical ratio of 0.78 (i.e.  $(3/5)^{1/2}$ ) for a homogeneous and dense sphere. This suggests a core-shell structure for the HPICs, the shell being swollen by water. Therefore, to get more information than the radius of gyration, SAXS intensity profiles were modelled using the form factor of polydisperse spherical core-shell particles (see Materials and Methods). In the insert of **Figure 6**, examples of such modelling are shown as well as the corresponding electron density profiles. The quality of the fitting strongly supports the assumption concerning the core-shell structures of the HPICs. All the parameters deduced from these fits are available in **Table S1**. **Table 1** lists structural data obtained for  $\rho = 1$ .

**Table 1.** Structural parameters deduced from DLS and SAXS experiments for Ga HPICs (at  $\rho = 1$ ).

Core radius <sup>b</sup>	External radius <sup>b</sup>	Gyration radius <sup>a</sup>	Hydrodynamic radius <sup>c</sup>
$R_c$ (nm)	$R_e$ (nm)	$R_g$ (nm)	$R_h$ (nm)
$4.3 \pm 0.9$	$11 \pm 3$	$7.5 \pm 0.4$	$11 \pm 3$

*deduced from SAXS experiments: a Guinier analysis, b model fitting; c deduced from DLS experiments*

SAXS experiments led to interesting structural information but the localization and density of the gallium ions remained unclear at this stage. Complementary to SAXS, anomalous small angle X-ray scattering measurements[30, 31] were then performed, since ASAXS is a method which is element sensitive. In **Figure 7**, the measured intensities for different values of the incident energy are reported for a Ga HPIC solution with  $\rho = 1$ . The intensity clearly varies with incident energy as it approaches the  $\text{Ga}^{3+}$  threshold. Such an energy dependence of the scattering intensity allows one to extract information about the gallium ion localization within the HPICs solution.

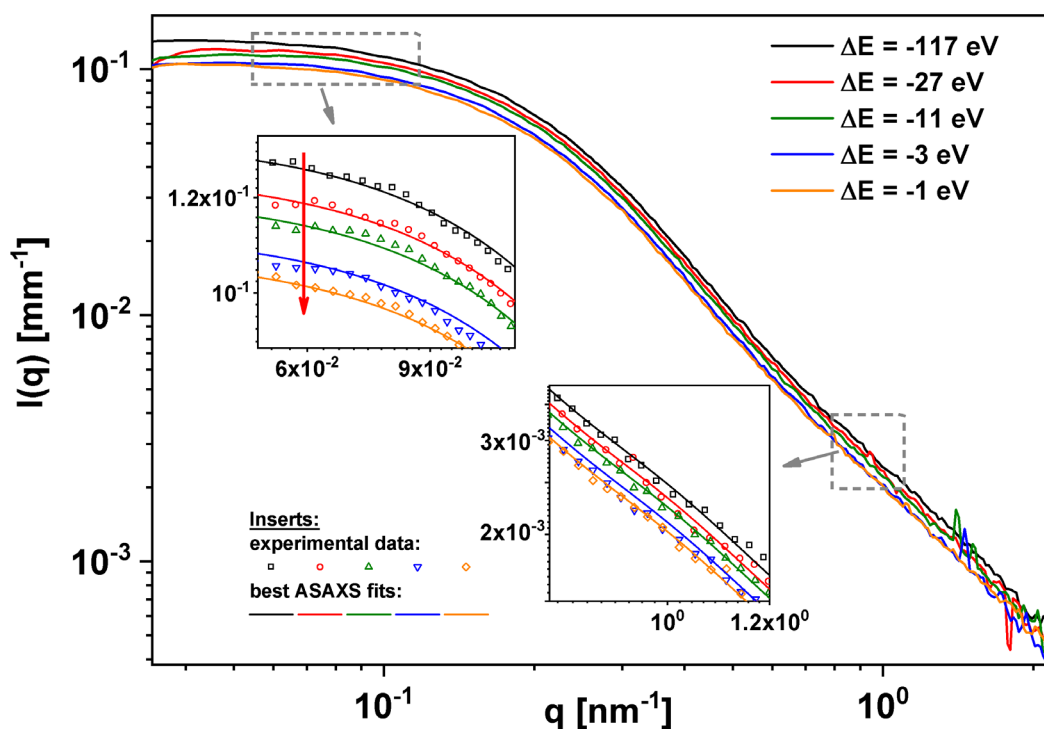


**Figure 7.** Scattered intensity versus the scattering wave vector  $q$ , as a function of the incident energy (HPIC solution with  $\rho = 1$  and pH 6.8). For clarity, only five energies are shown, corresponding to the difference  $\Delta E$  to the absorption K-edge of  $\text{Ga}^{3+}$  counterions: -117 eV, -27 eV, -11 eV, -3 eV and -1 eV. **Inserts.** Results of direct modelling of the ASAXS data presented in two magnified views: the relative change of the scattered intensity at the different energies directly depends on the number of the bound ions and allows to determine the density of the gallium ions. The arrow is a guide for the eyes illustrating the intensity change while approaching the energy of the absorption edge of Ga.

Firstly, decomposition of the ASAXS signal from a Ga HPIC solution ( $\rho = 1$  at pH 6.8) was obtained according to **Eq. 7** and is shown in **Figure 8**. The term  $F_0^2(q)$  (i.e. the non-resonant intensity due to the polymer mainly) and the term  $v^2(q)$  (i.e., the energy dependent resonant term related to the gallium) have similar  $q$  dependence. This indicates that the spatial distribution of both the copolymers and the counterions within the HPICs has a similar dependence on the radial distance  $r$ . For information, the  $F_0(q)v(q)$  cross-term (deduced from the decomposition of the ASAXS signal and containing information about both the resonant and non-resonant terms) is also plotted in **Figure 8**.

The individual contributions of the non-resonant (spherical nano-objects) and the resonant ( $\text{Ga}^{3+}$  counterions) terms are represented for different ratios  $\rho$  in **Figure S4**. The resonant term  $v^2(q)$ , originating from the localized  $\text{Ga}^{3+}$  counterions, becomes weaker as  $\rho$  decreases. Simultaneously, SAXS data present a characteristic polyelectrolyte peak and an intensity upturn at low- $q$  for  $\rho < 0.8$ . Therefore,  $\text{Ga}^{3+}$  counterions are not localized anymore and may diffuse freely in the solution without any particular structural organization. The counterion condensation is only detected once the nano-objects are structured. Such a behavior is in agreement with the previous results obtained by NMR, stopped-flow and DLS experiments.

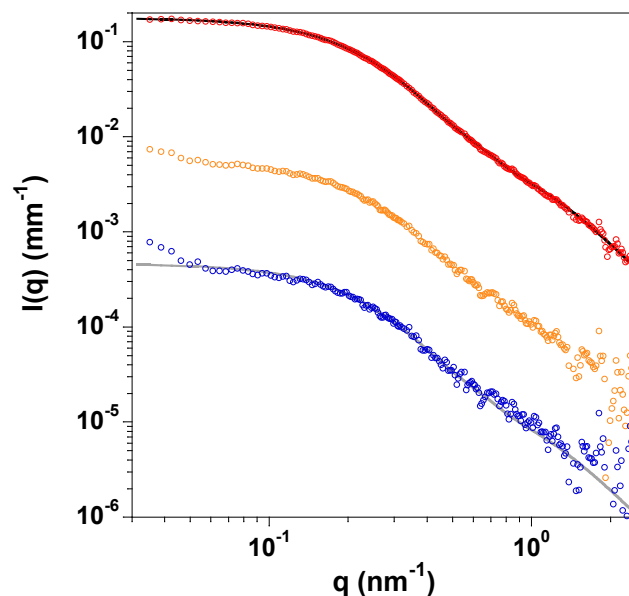


**Figure 8.** Decomposition of the measured ASAXS intensity according to **Eq. 7**, for a Ga HPIC solution ( $\rho = 1$  at pH 6.8). In red (upper curve), the  $F_0^2(q)$  term. In orange (middle curve), the  $F_0(q) \cdot v(q)$  term. In blue (lower curve), the  $v^2(q)$  term. The solid line represents the best SAXS fit to **Eq. 4** as already presented in **Figure 6**. It has been scaled down (grey line) as guide to the eye to the intensity of the  $v^2(q)$  term, to illustrate the similarity in the  $q$  dependence.

Secondly, in order to derive quantitative information about the distribution of the Ga ions, simultaneous fitting of the ASAXS datasets recorded at several energies was performed. More details about the used model can be found in the Materials and Methods section.

**Figure 7** shows the best result of the modellization, according to **Eq. 8**, performed on the scattering curves measured at -117 eV, -27 eV, -11 eV, -3 eV and -1 eV below the absorption edge. The relative change of the scattered intensity at the different energies directly depends on the number of the bound ions and allows to determine the density of the gallium ions,  $d_{\text{Ga}}$ , in the system without further assumptions. This is shown for the sake of clearness for two selected  $q$  ranges in the insets of **Figure 7**.

According to the ASAXS modelling, Ga ions are concentrated in the core. However, a small fraction of counterions (ca 7%) is also present at the interface and along the PEO chains. It should be noted that the presence of  $\text{Ga}^{3+}$  ions in the PEO shell may simply be related to a slight excess of ions compared to the electroneutrality. This is related to the somewhat poor accuracy of the ratio  $\rho$  due to the slight polydispersity of the copolymer. One can safely conclude that, at  $\rho = 1$ , the nano-objects present a core rich in PAA polyions. The counterion distribution in the core and shell shows density fluctuations, i.e. an organization into ion-rich/ion-poor regions (“blobs”), the nature of which, however, cannot be determined from the fitted Ornstein-Zernike term. The presence of an Ornstein-Zernike contribution in the SAXS signal (non-resonant term) also indicates the presence of PAA rich (or poor) zones in the core and of PEO respectively in the shell.

Finally, the aggregation number  $N_{\text{agg}}$  (i.e. the average number of macromolecules associated in one hybrid micelle) can be estimated from the SAXS and ASAXS results.

Indeed, assuming that the core of the HPICs has a density similar to that of polyacrylate or zinc diacrylate (data available in the literature - unfortunately no information concerning a theoretical gallium triacrylate was found-),  $N_{\text{agg}}$  can be calculated from the following equation:

$$N_{\text{agg}} = (4/3\pi) N_{\text{av}} R_c^3 \cdot d_{\text{AA}}/M_{\text{PAA}} \quad (\text{Eq. 10})$$

where  $N_{av}$  is the Avogadro's number,  $M_{PAA}$  is the molar mass of the PAA block i.e. 3.2 kg/mol,  $d_{AA}$  the hypothetical density of the HPIC core (ca  $1.3 \pm 0.1$ ).

This leads to an estimate of  $N_{agg}$  around 80 for  $R_c = 4.3$  nm. Since the  $R_c$  value (mean 4.3 nm, standard deviation 0.9 nm) lies most probably between 3.4 nm (4.3-0.9 nm) and 5.2 nm (4.3+0.9 nm),  $N_{agg}$  should likely be in the 40-140 range. This estimated value is not far from the one already calculated for other HPIC systems. Indeed, the association between poly(sodium(sulfamate-carboxylate)isoprene)<sub>18.9k</sub>-*block*-poly(ethylene oxide)<sub>14.8k</sub> and cadmium ions was described with an aggregation number around 90.[32] This is also close to the 40-70 aggregation number reported for complex coacervates micelles obtained with two block copolyelectrolytes.[33] Y.-H. Jong et al. have estimated that ca 80 to 390 platinum ions were trapped in the polymeric structure formed with poly(acrylic acid)-*block*-poly(ethylene glycol methacrylate) or poly(acrylic acid)-*block*-poly(ethylene glycol).[34] In our case, an aggregation number of 80 suggests that about 1100 Ga ions are trapped on average in one hybrid micelle: the Ga density should therefore be around 3.4 ions per nm<sup>3</sup> in the core or 0.2 ion per nm<sup>3</sup> in the full nano-object. For comparison, in a previous system with HPICs formed with copper ions,[29] Cu HPICs were found by SAXS (data not shown) with a smaller core radius of 3.2 nm: aggregation number is then estimated close to 33 and the number of copper per micelle around 690. We must underline that 3.4 ions per nm<sup>3</sup> is a rough estimation of the Ga density due to the error in the core radius and the uncertainty in the density of the AA chains in the core,  $d_{AA}$ .

Complementarily, as already stated, fitting of the ASAXS curves offers a direct means to determine the density of the Ga ions and therefore to estimate the aggregation number. Indeed, the relative change of the scattered intensity at the different energies directly depends on the number of bound ions and enables determining the density of the gallium ions,  $d_{Ga}$ , in the system without further assumptions.  $d_{Ga}$  was found around  $5 \pm 1$  ions per nm<sup>3</sup> (i.e. ca 1700 ions per HPIC). This is slightly higher than the previous estimation (3.4 ions per nm<sup>3</sup> see above). Assuming a  $DP_n$  of 44 for the PAA block and 3 carboxylate functions per gallium, this leads to an evaluation of the aggregation number of the HPICs around 120 and most probably in the 60-180 range. The large error originated from the 20% of error on the value of  $R_c$ .

### Stability of the Ga HPICs with pH

The colloidal stability of the Ga HPICs is ensured by the PEO shell which explains the near zero zeta potential of these nano-objects. As shown for previous HPICs, one of the principal factors that can destabilize the object is the pH. Indeed, the protonation of the carboxylate groups of the copolymer induces release of the metal ions and disassociation of the copolymer chains. In the case of Ga HPICs, this is easily observed by DLS experiments (see **Figure 9**).



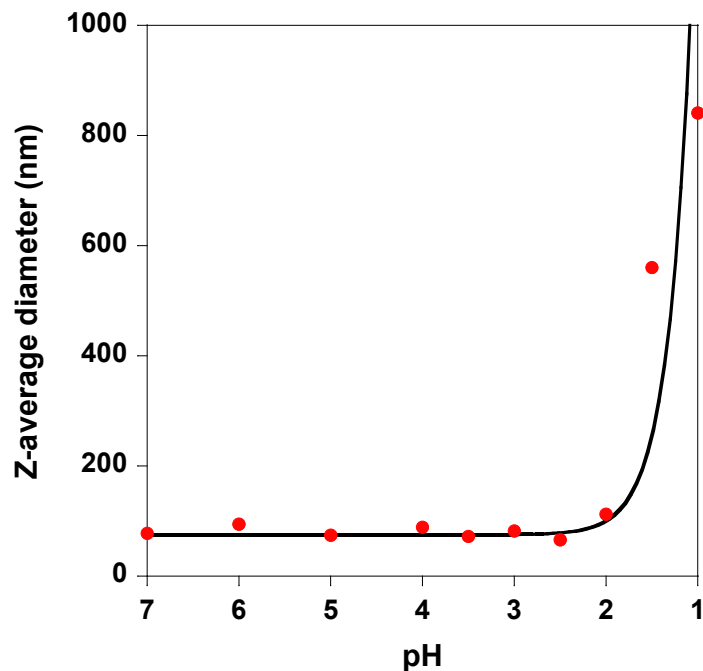


**Figure 9.** Evolution of the Z-average diameter of the Ga HPICs ( $\rho = 1$ ) as a function of the pH of the solution (starting at a pH close to 7). The solid line is just a guide for the eyes.

When the pH of the Ga HPIC solution decreased, no change in the Z-average size of the nano-objects was observed until pH 2. Then, below pH 2, a large increase of this average size demonstrated the change of structure of the HPICs. As mentioned above, the apparent increase in size may be due to poorly defined association of free copolymers either because of a lower solubility due to their neutralization or to interactions through free gallium ions. This change is recorded for a much lower pH than that of gadolinium HPICs.[18] This shows that the interaction between gallium and carboxylates is much stronger than the one between gadolinium and carboxylates. This behavior is similar to that observed with zirconium ions.[17]

As a further evidence, structural investigations by ASAXS were also performed with decreasing pH from 6.8 to 2. Disaggregation was observed for a value of pH equal to 2 with a transition from globule to coil structure (**Figure S5**). The value of the radius of gyration drops from 7.5 to 2.7 nm, the latter corresponding to the average coil size of the block copolymer. Counterion condensation is observed for pH 6.8 and 4.0, as shown in **Figure S6**. Again, the same dependence on the radial distance  $r$  is observed for the counterions and the polyion at the different pHs. At pH 2, counterions appear to be free, as no  $q$  dependence of the resonant scattering can be determined.

## CONCLUSION

This work has demonstrated that addition of gallium ions to a PEO<sub>5k</sub>-PAA<sub>3.2k</sub> block copolymer solution led to the formation of well-defined nano-objects having a core-shell structure. These nano-objects are rapidly in equilibrium and start to form only when the charge ratio,  $\rho$ , between the positive gallium ions and the negative PAA polyanions is higher than 0.6-0.7. At charge stoichiometry ( $\rho = 1$ ), all gallium ions and polymers form electroneutral HPICs. These nano-objects present a core-shell structure with a very low polydispersity in size. The core contains gallium interacting with the carboxylate functions in a somewhat rigid architecture (at the time scale of the NMR). The shell made of PEO is relatively free to move. The core-shell structure has an overall radius around 11 nm with a core radius close to 4.5 nm. Roughly speaking, each HPIC contains around 100 polymers and 1400 gallium ions. These studies demonstrate, in particular, the utility of ASAXS for tracking inorganic ions in the solution or within the nano-objects and for corroborating data obtained with other techniques. Further

studies with other polymers are in progress in order to improve the chemical stability of the nano-object in solution at various pHs. The biocompatibility of Ga HPICs is also currently under study. Using radioactive  $^{68}\text{Ga}$  ions, the Ga HPICs will then be used as radiopharmaceutical for positron emission tomography imaging. Such application of Ga HPICs will be assessed *in vivo* in the mouse.

## ACKNOWLEDGEMENTS

The authors thank the “Agence Nationale pour la Recherche” for funding (ANR Hybrid MRI, n° ANR-19-CE09-0011-01) as well as Toulouse Tech Transfer and Region Occitanie (FESR\_PREMAT-000025/prématuration 2017 Hybrid-MRI) for financial support. ESRF is acknowledged for provision of beamtime on the ID02 beamline. The authors wish also to thank Dr. Baptiste Amouroux and Kamilia Ayadi for various experiments.

## REFERENCES

- [1] X.M. Ge, M.Y. Wei, S.N. He, W.E. Yuan, Advances of Non-Ionic Surfactant Vesicles (Niosomes) and Their Application in Drug Delivery, *Pharmaceutics* 11(2) (2019).
- [2] R. Nagarajan, Self-Assembly: From Surfactants to Nanoparticles, Wiley Series on Surface and Interfacial Chemistry, Wiley, 2019, p. 368.
- [3] N.A. Lynd, A.J. Meuler, M.A. Hillmyer, Polydispersity and block copolymer self-assembly, *Progress in Polymer Science* 33(9) (2008) 875-893.
- [4] M. Dionzou, A. Morere, C. Roux, B. Lonetti, J.D. Marty, C. Mingotaud, P. Joseph, D. Goudouneche, B. Payre, M. Leonetti, A.F. Mingotaud, Comparison of methods for the fabrication and the characterization of polymer self-assemblies: what are the important parameters, *Soft Matter* 12(7) (2016) 2166-2176.
- [5] D. Chandler, Interfaces and the driving force of hydrophobic assembly, *Nature* 437(7059) (2005) 640-647.
- [6] I.K. Voets, A. de Keizer, M.A.C. Stuart, Complex coacervate core micelles, *Advances in Colloid and Interface Science* 147-48 (2009) 300-318.
- [7] M. Abbas, W.P. Lipin, J. Wang, E. Spruijt, Peptide-based coacervates as biomimetic protocells, *Chem. Soc. Rev.* 50(6) (2021) 3690-3705.
- [8] X.Q. Liu, J.P. Chapel, C. Schatz, Structure, thermodynamic and kinetic signatures of a synthetic polyelectrolyte coacervating system, *Advances in Colloid and Interface Science* 239 (2017) 178-186.
- [9] B. Schmidt, Double Hydrophilic Block Copolymer Self-Assembly in Aqueous Solution, *Macromol. Chem. Phys.* 219(7) (2018).
- [10] A. El Jundi, S.J. Buwalda, Y. Bakkour, X. Garric, B. Nottelet, Double hydrophilic block copolymers self-assemblies in biomedical applications, *Advances in Colloid and Interface Science* 283 (2020).
- [11] Z. Lu, Y. Yin, Colloidal nanoparticle clusters: functional materials by design, *Chem. Soc. Rev.* 41(21) (2012) 6874-6887.
- [12] M. Yokoyama, T. Okano, Y. Sakurai, S. Suwa, K. Kataoka, Introduction of cisplatin into polymeric micelle, *Journal of Controlled Release* 39(2) (1996) 351-356.
- [13] L. Volkmann, M. Köhler, F.H. Sobotta, M.T. Enke, J.C. Brendel, F.H. Schacher, Poly(2-acrylamidoglycolic acid) (PAGA): Controlled Polymerization Using RAFT and Chelation of Metal Cations, *Macromolecules* 51(18) (2018) 7284-7294.
- [14] N. Sanson, F. Bouyer, M. Destarac, M. In, C. Gérardin, Hybrid Polyion Complex Micelles Formed from Double Hydrophilic Block Copolymers and Multivalent Metal Ions: Size Control and Nanostructure, *Langmuir* 28(8) (2012) 3773-3782.
- [15] H.W. Shin, H. Sohn, Y.H. Jeong, S.M. Lee, Construction of Paramagnetic Manganese-Chelated Polymeric Nanoparticles Using Pyrene-End-Modified Double-Hydrophilic Block Copolymers for Enhanced Magnetic Resonance Relaxivity: A Comparative Study with Cisplatin Pharmacophore, *Langmuir* 35(19) (2019) 6421-6428.

- [16] K.H. Markiewicz, L. Seiler, I. Misztalewska, K. Winkler, S. Harrison, A.Z. Wilczewska, M. Destarac, J.D. Marty, Advantages of poly(vinyl phosphonic acid)-based double hydrophilic block copolymers for the stabilization of iron oxide nanoparticles, *Polymer Chemistry* 7(41) (2016) 6391-6399.
- [17] M. Yon, S. Gineste, G. Parigi, B. Lonetti, L. Gibot, D.R. Talham, J.-D. Marty, C. Mingotaud, Hybrid Polymeric Nanostructures Stabilized by Zirconium and Gadolinium Ions for Use as Magnetic Resonance Imaging Contrast Agents, *ACS Applied Nano Materials* (2021).
- [18] C. Frangville, Y. Li, C. Billotey, D.R. Talham, J. Taleb, P. Roux, J.-D. Marty, C. Mingotaud, Assembly of Double-Hydrophilic Block Copolymers Triggered by Gadolinium Ions: New Colloidal MRI Contrast Agents, *Nano Letters* 16(7) (2016) 4069-4073.
- [19] T. Narayanan, M. Sztucki, P. Van Vaerenbergh, J. Leonardon, J. Gorini, L. Claustre, F. Sever, J. Morse, P. Boesecke, A multipurpose instrument for time-resolved ultra-small-angle and coherent X-ray scattering, *Journal of Applied Crystallography* 51(6) (2018) 1511-1524.
- [20] P. Boesecke, Reduction of two-dimensional small- and wide-angle X-ray scattering data, *Journal of Applied Crystallography* 40(s1) (2007) s423-s427.
- [21] SAXSutilities. Available online: <http://www.saxsutilities.eu>.
- [22] A. Guinier, G. Fournet, *Small-Angle Scattering of X-Rays*, John Wiley & Sons, New York, 1955.
- [23] A. Jusufi, M. Ballauff, Correlations and Fluctuations of Charged Colloids as Determined by Anomalous Small-Angle X-Ray Scattering, *Macromolecular Theory and Simulations* 15(3) (2006) 193-197.
- [24] M. Sztucki, E. Di Cola, T. Narayanan, Instrumental developments for anomalous small-angle X-ray scattering from soft matter systems, *Journal of Applied Crystallography* 43(6) (2010) 1479-1487.
- [25] N. Dingenouts, M. Patel, S. Rosenfeldt, D. Pontoni, T. Narayanan, M. Ballauff, Counterion Distribution around a Spherical Polyelectrolyte Brush Probed by Anomalous Small-Angle X-ray Scattering, *Macromolecules* 37(21) (2004) 8152-8159.
- [26] M. Muthukumar, Ordinary–extraordinary transition in dynamics of solutions of charged macromolecules, *Proceedings of the National Academy of Sciences* 113(45) (2016) 12627.
- [27] F. Kuehn, K. Fischer, M. Schmidt, Kinetics of Complex Formation between DNA and Cationically Charged Cylindrical Brush Polymers Observed by Stopped Flow Light Scattering, *Macromolecular Rapid Communications* 30(17) (2009) 1470-1476.
- [28] J.D. Glickson, T.P. Pitner, J. Webb, R.A. Gams, Hydrogen-1 and gallium-71 nuclear magnetic resonance study of gallium citrate in aqueous solution, *Journal of the American Chemical Society* 97(7) (1975) 1679-1683.
- [29] M. Mestivier, J.R. Li, A. Camy, C. Frangville, C. Mingotaud, F. Benoit-Marquie, J.D. Marty, Copper-Based Hybrid Polyion Complexes for Fenton-Like Reactions, *Chemistry-a European Journal* 26(62) (2020) 14152-14158.
- [30] M. Sztucki, E. Di Cola, T. Narayanan, Anomalous small-angle X-ray scattering from charged soft matter, *The European Physical Journal Special Topics* 208(1) (2012) 319-331.
- [31] M. Sztucki, E. Di Cola, T. Narayanan, New opportunities for Anomalous Small-Angle X-Ray Scattering to characterize Charged Soft Matter Systems, *Journal of Physics: Conference Series* 272 (2011) 012004.
- [32] M. Uchman, K. Procházka, K. Gatsouli, S. Pispas, M. Špírková, CdS-containing nano-assemblies of double hydrophilic block copolymers in water, *Colloid and Polymer Science* 289(9) (2011) 1045-1053.
- [33] C.C.M. Sproncken, J.R. Magana, I.K. Voets, 100th Anniversary of Macromolecular Science Viewpoint: Attractive Soft Matter: Association Kinetics, Dynamics, and Pathway Complexity in Electrostatically Coassembled Micelles, *Acs Macro Letters* 10(2) (2021) 167-179.
- [34] Y.-H. Jeong, H.-W. Shin, J.-Y. Kwon, S.-M. Lee, Cisplatin-Encapsulated Polymeric Nanoparticles with Molecular Geometry-Regulated Colloidal Properties and Controlled Drug Release, *ACS Applied Materials & Interfaces* 10(28) (2018) 23617-23629.